Oscillatory biquadratic coupling in Fe/Cr/Fe(001)

A. J. R. Ives, J. A. C. Bland, R. J. Hicken, and C. Daboo
Cavendish Laboratory, University of Cambridge, Madingley Road, Cambridge CB3 0HE, United Kingdom
(Received 13 August 1996; revised manuscript received 3 December 1996)

Polar Kerr measurements have been used to measure the dependence of the biquadratic coupling strength B_{12} on Cr thickness in an Fe/Cr/Fe trilayer. The overall behavior, which consists of a maximum coupling strength at $d_{Cr}=5$ Å (3.5 ML) with a falloff at greater Cr thicknesses, is found to be consistent with in-plane Kerr and Brillouin light-scattering measurements performed on the same sample. The polar Kerr measurements suggest additionally that B_{12} increases from zero near zero Cr thickness, and that it oscillates in magnitude after the first peak, with a second peak in B_{12} occurring at about $d_{Cr}=12$ Å (8.3 ML). The positions and heights of the first and second biquadratic coupling maxima, in relation to the first bilinear coupling maximum, show excellent agreement with previous measurements by Köbler *et al.* of the biquadratic coupling behavior in Fe/Cr/Fe, and also show good agreement with the predictions of an intrinsic biquadratic coupling mechanism due to Edwards *et al.* [S0163-1829(97)09117-0]

I. INTRODUCTION

Antiferromagnetic (AFM) interlayer exchange coupling was discovered in Fe/Cr/Fe structures by Grünberg *et al.*,[1] and the Fe/Cr system has since become particularly important to the development of our understanding of the mechanism of interlayer exchange coupling.[2] Chromium is an interesting choice of spacer material because bulk Cr is known to exhibit incommensurate spin-density-wave antiferromagnetism.[3] Fe/Cr structures grown on Fe(001) whiskers are believed to have the flattest interfaces currently obtainable, and it was in such structures that the interlayer coupling was observed to oscillate with a period of approximately two Cr monolayers (ML) in addition to the previously discovered long-period oscillations of about 18 Å (12.5 ML).[4,5] It was subsequently demonstrated that these short-period coupling oscillations are correlated with the AFM ordering of the Cr.[6] There is now general agreement that the period of the coupling oscillations is determined by the geometry of the Fermi surface of the spacer material in the direction perpendicular to the layers, so that the discovery by Fullerton *et al.*[7] that spacer layers of two different orientations yielded identical values for the strength, oscillation period and phase of the long-period oscillations was somewhat surprising. Studies using Fe whisker substrates have provided information concerning the phase of the short-period oscillations.[8] Since an odd number of Cr monolayers are expected to cause ferromagnetic alignment of adjacent Fe layers, the observation by Heinrich *et al.*[8] and by Unguris, Celotta, Pierce[6] of AFM coupling after the growth of 5 ML (~ 7 Å) of Cr grown on Fe whisker samples was again surprising, and is associated with a phase slip of the AFM ordering of the Cr. Recent studies of the Fe-Cr interface using scanning tunneling microscopy[9] (STM) and angle-resolved Auger spectroscopy[10] show that strong exchange interdiffusion of Fe and Cr occurs. This process may be responsible for the phase slip observed at low Cr thicknesses, a view which is supported by calculations of exchange coupling in intermixed Fe/Cr interfaces using a tight-binding scheme.[11]

The usual bilinear coupling is proportional to the cosine of the angle between the magnetizations $\mathbf{M}_1$ and $\mathbf{M}_2$ of adjacent ferromagnetic layers, and has the form $-2A_{12}\hat{\mathbf{M}}_1\cdot\hat{\mathbf{M}}_2$, where $\hat{\mathbf{M}}_1$ and $\hat{\mathbf{M}}_2$ are unit vectors along the directions of $\mathbf{M}_1$ and $\mathbf{M}_2$. It is known that there may also exist a so-called biquadratic interlayer coupling which is proportional to the cosine of the angle squared and can favor a 90° alignment of the magnetizations of the ferromagnetic layers. The biquadratic coupling energy has the form $-2B_{12}(\hat{\mathbf{M}}_1\cdot\hat{\mathbf{M}}_2)^2$. Biquadratic coupling was discovered in Fe/Cr/Fe(001) magnetic trilayers by Rührig *et al.*[12] using magneto-optic Kerr effect microscopy, and has since been found to occur in a number of other systems, such as Fe/(Al,Au)/Fe(001),[13] Fe/(Cu,Ag)/Fe(001),[14] and NiFe/Ag/NiFe.[15] The biquadratic coupling strength in Fe/Cr/Fe structures has been observed to be of comparable magnitude to the bilinear coupling strength.[8,16]

Several theories have been proposed to account for the biquadratic coupling, some of which are intrinsic to the electronic structure of the multilayer system, and are referred to as intrinsic theories, and some of which rely on effects other than the electronic structure, such as structural imperfections, and are referred to as extrinsic theories. Three intrinsic theories due to Edwards, Ward, and Mathon,[17] Barnaś,[18] and Erickson, Hathaway, and Cullen[19] predict that the biquadratic coupling oscillates as a function of interlayer thickness and decays in amplitude with increasing interlayer thickness in a similar way to the bilinear coupling. In all of Refs. 17–19, the phase and period of the biquadratic oscillations are found to be different from those of the bilinear coupling oscillations, and the amplitude of the biquadratic coupling is found to be much lower than that of the bilinear coupling. A problem with some of the intrinsic theories has been that the size of the biquadratic coupling predicted is too small to account for the experimentally observed values,[17,18] and in some cases it is too small by orders of magnitude.[19–21] A consequence of the different phase and period of the biquadratic coupling is that at certain interlayer thicknesses, where the bilinear coupling passes through zero, the biquadratic

coupling may be larger than the bilinear coupling, even when the amplitude of the oscillations in the biquadratic coupling is many times smaller than it is for the bilinear coupling. One extrinsic theory due to Demokritov *et al.*,[22] in which biquadratic coupling arises as a result of the magnetic-dipole field created by magnetic layers with roughness, predicts an exponential falloff of the biquadratic coupling with no oscillation as a function of interlayer thickness.

Two well-known theories of biquadratic coupling are those of Slonczewski. The first of these, called the fluctuation mechanism, is an extrinsic mechanism associated with spatial fluctuations of bilinear coupling due to terraced variations of spacer thickness in nonideal specimens with roughness.[23] The second is an intrinsic mechanism, called the loose-spins model, which postulates that the biquadratic exchange coupling is mediated by localized atomic-electron states at the interfaces of the spacer layer.[24] Both these theories were shown to predict magnitudes of biquadratic coupling strengths that were in good agreement with experimentally observed values. Very strong near-90° coupling has recently been reported in CoFe/Mn/CoFe sandwich structures, without any evidence for bilinear coupling.[25] In this case, the field dependence of the magnetization was found to be well fitted by an extrinsic model assuming a type of coupling energy of the form $E=C_+(\phi_1-\phi_2)^2+C_-(\phi_1-\phi_2-\pi)^2$.

So far, while many theories have been proposed to account for the biquadratic coupling, very little experimental data has been published to show how the biquadratic coupling varies in strength with nonmagnetic interlayer thickness in real magnetic/nonmagnetic multilayer systems. In the present paper, we seek to redress this imbalance by describing how polar Kerr measurements have been used to investigate the dependence of the biquadratic coupling on Cr interlayer thickness in a Fe/Cr/Fe trilayer grown on Ag/GaAs(001). The Cr thickness dependence of the biquadratic coupling obtained using polar Kerr measurements is compared first with previously published estimates of the biquadratic coupling strength obtained from in-plane Kerr and Brillouin light-scattering (BLS) measurements on the same sample;[26] second, with the published experimental results of Köbler *et al.*;[16] and finally with the results of a theoretical analysis by Edwards, Ward, and Mathon[17] arising from an intrinsic biquadratic coupling mechanism.

The Fe/Cr/Fe trilayer studied here was grown with structure Cr(20 Å)/Fe(20 Å)/Cr(0–40 Å)/Fe(20 Å)/Ag(600 Å)/Fe(15 Å)/GaAs(001). The Cr spacer layer was grown with the substrate held at room temperature. Although this is known to result in less well-defined interfaces and in the suppression of the short-wavelength oscillations in A_{12}, such structures can offer valuable insights into the origin of the coupling behavior. In particular, the comparison with the behavior obtained for structures prepared at elevated temperature is important. The procedures used for the ultrahigh vacuum growth of the trilayer, together with easy-axis in-plane Kerr magnetization curves and BLS measurements obtained as a function of Cr thickness, have been described previously in Ref. 26. The variation of the in-plane easy-axis saturation field with Cr thickness, showing the oscillatory nature of the coupling, has however been reproduced again in Fig. 1(a), since it will be needed for comparison with the

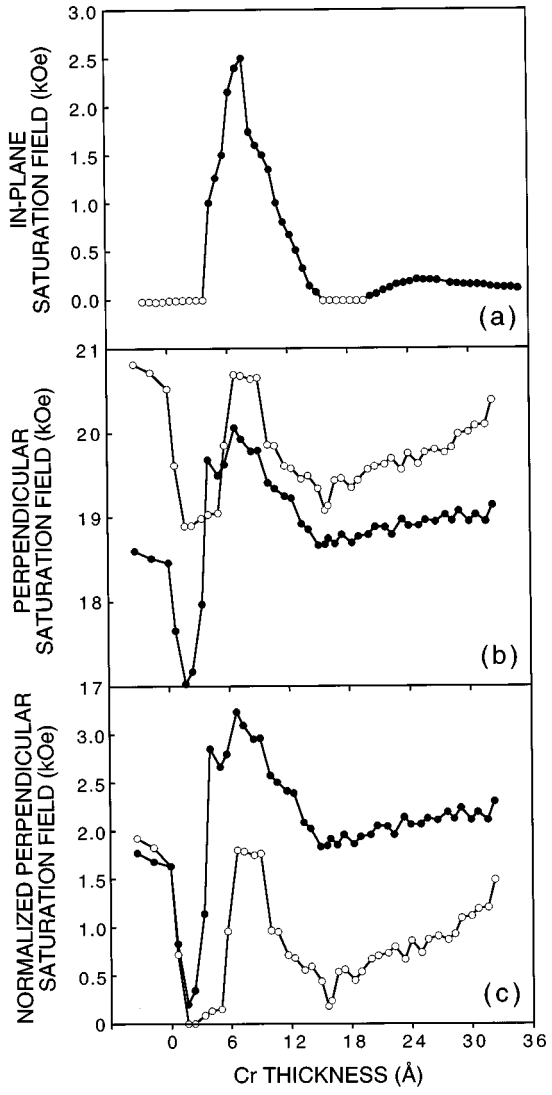

FIG. 1. (a) The in-plane easy axis saturation field as determined from in-plane Kerr magnetometry is plotted as a function of Cr thickness for the trilayer. (b) The perpendicular saturation fields $H_s^{\perp}$ (closed circles) and $H_s^{\chi\perp}$ (open circles) are plotted versus Cr interlayer thickness for the trilayer. (c) The normalized perpendicular saturation fields $\Delta H_s^{\perp}$ (closed circles) and $\Delta H_s^{\chi\perp}$ (open circles) are plotted versus Cr interlayer thickness for the trilayer.

polar Kerr data. Two regions of AFM coupling exist: the first extends from a Cr thickness of 4 Å (2.8 ML) to 15 Å (10.4 ML), while the second begins at a Cr thickness of 20 Å (13.9 ML) and continues to the end of the wedge where the Cr layer is 40 Å (27.8 ML) thick. The form of the coupling is predominantly due to the long-period coupling oscillations, but vestiges of the short period coupling may be seen as shoulders on both sides of the main AFM coupling peak at 7 Å (4.9 ML). From the separation of the maxima of the first and second bilinear coupling peaks in Fig. 1(a), a value of about 18 Å (12.5 ML) was obtained for the long period of oscillation in the coupling, which agreed well with the value of 12 ± 1 ML (17.3 ± 1.4 Å) deduced by Pierce *et al.*[27] for samples grown on Fe whisker substrates. For Cr thicknesses less than 4 Å (2.8 ML) and between 16 and 20 Å (11.1 and 13.9 ML), the easy-axis loops are square, indicating that the

Fe layers are either ferromagnetically (FM) coupled or uncoupled.

II. POLAR KERR MAGNETOMETRY

Polar Kerr magnetization curves were obtained as a function of Cr thickness from the Fe/Cr/Fe trilayer using an experimental arrangement shown in Ref. 28. For the 20-Å Cr layers in the sample studied here, the normal to the film surface is a hard direction of magnetization so that large applied fields are necessary to saturate the Fe layers in the perpendicular direction. The analysis of the polar Kerr magnetization curves is thus simplified by the fact that magnetization can nearly always be assumed to proceed by coherent rotation, and by the fact that the remanence is always zero or almost zero.

The 12 mm long sample was placed in air and at room temperature at the end of an insert tube, close to the center of a 7 T superconducting magnet, with the magnetic field directed perpendicular to the sample surface. An intensity stabilized He-Ne laser beam was focused on the sample down to a spot size of 0.2 mm, at near normal incidence, and moved across it using a plane and a concave mirror both mounted on a micrometer stage. This arrangement was designed so that the laser light did not have to pass through any windows or lenses in the vicinity of the field, thus eliminating problems due to Faraday rotation or birefringence. Polar Kerr measurements were performed as a function of position along the wedge in order to sample the magnetization curves at the different Cr interlayer thicknesses. Nearly all the perpendicular magnetization curves obtained using the polar Kerr effect have a background contribution which varies linearly with field, and which is always subtracted off before the curves are normalized to the saturation value of the magnetization. In addition, a very slight distortion of the magnetization curves can occur because the relationship between the intensity recorded after the analyzing polarizer and the magnetization, is not perfectly linear. This distortion is assumed to have a negligible affect on the magnetization curves for the purposes of the analysis carried out here.

The conventional perpendicular saturation field $H_s^{\perp}$ has been estimated for the wedged trilayer by taking the intersection of the perpendicular magnetization curve with $M/M_s=\alpha$, where α is chosen to be the highest value of M/M_s at which the values of $H_s^{\perp}$ obtained for all thicknesses of the wedged layer are not seriously affected by noise in the magnetization curves (see Refs. 28, 29), and for the Fe/Cr/Fe trilayer α has been chosen to have the value 0.96. This procedure was necessary because of the asymptotic approach of the magnetization to saturation and because of noise fluctuations in the data, although it does lead to $H_s^{\perp}$ being an underestimate of the true saturation field. As in Refs. 28 and 29, a second saturation field $H_s^{\chi\perp}=1/\chi_0$ has also been used to analyze the magnetization curves, where χ_0 is the initial magnetization gradient of the perpendicular magnetization curve calculated using reduced units of M/M_s. Evaluating this saturation field should, in principle, allow further information to be extracted from the perpendicular magnetization curve, as its dependence on the quantities which vary with the wedge thickness is different from that of $H_s^{\perp}$.

The perpendicular saturation fields $H_s^{\perp}$ and $H_s^{\chi\perp}$ obtained from the polar Kerr magnetization curves are plotted in Fig. 1(b). For the first three data points on the left-hand side of the plots of $H_s^{\perp}$ and $H_s^{\chi\perp}$ the Cr interlayer has zero thickness so the effective Fe layer thickness is 40 Å. The Cr wedge begins after the third data point, and between the third and fifth points $H_s^{\perp}$ and $H_s^{\chi\perp}$ both fall abruptly by about 1.6 kOe. As a partial layer of Cr is introduced into the middle of the 40 Å Fe layer, the saturation field decreases due to the increased interface anisotropy fields associated with the extra interfaces with the Cr layer. The saturation field continues to decrease with Cr spacer thickness until antiferromagnetic coupling begins to be established.

It is interesting to note that a minimum in the saturation field occurs at approximately 1 ML (1.44 Å) Cr thickness. Davies *et al.*[9] deduced that FM coupling persists up to $\sim$3 ML (4.3 Å) Cr thickness but were unable to probe the variation in coupling strength since no fields could be applied in the scanning electron microscopy with polarization analysis experiment that they performed. For a sharp interface, ferromagnetic coupling of the Fe layers would be expected to occur at a Cr thickness of 1 ML since a monolayer of Cr is thought to order antiferromagnetically with a neighboring Fe layer.[30] However, the STM and Auger spectroscopy studies in Refs. 9 and 10, respectively, indicate that the spacer layer will correspond to a mixture of Cr and Fe at $\sim$1 ML thickness. Stoeffler and Gautier[11] have shown that for a 2 ML (2.88 Å) period ordered alloy, consisting of alternating layers of $Fe_{0.75}Cr_{0.25}$ and $Fe_{0.25}Cr_{0.75}$, the layers are ferromagnetically aligned. Thus the minimum we observe in the polar saturation field at 1 ML is likely to be due to ferromagnetic coupling between the Fe layers mediated by a ferromagnetically aligned FeCr spacer layer of monolayer thickness. For growth close to room temperature, only the first Cr layer is significantly intermixed according to the Auger spectroscopy studies of Heinrich *et al.*[10] Our results show that as the spacer thickness is further increased beyond 1 ML, the ferromagnetic coupling strength is rapidly reduced, first becoming AF at about 2.8 ML (4 Å). This is consistent with a corresponding rapid increase in the Cr concentration of the spacer layer, as expected from the intermixing studies for Cr growth close to room temperature. The second and successive Cr layers within the spacer should be almost 100% Cr and therefore the antiferromagnetic ordering will become established, while the moment of the first Cr layer will remain parallel to the bottom Fe layer magnetization. This leads to short-period oscillations in the coupling strength which are only weakly seen in our sample due to the rougher interfaces in comparison with those of structures grown at elevated temperatures. The existence of such an intermixed first layer is consistent with the phase slip which leads to the peak in the bilinear coupling occurring at 5 ML ($\sim$7 Å), seen more clearly in Fe-whisker samples with near-perfect interfaces.[6,8]

It should be noted that the behavior of the perpendicular saturation fields we observe is strikingly different from that of the easy-axis in-plane saturation field in Fig. 1(a), for which only a small change in the coercive field was observed at the start of the Cr wedge. The dramatic fall in saturation field observed using polar Kerr magnetometry shows that this technique is far more sensitive to the effect of a

magnetic/nonmagnetic interface than the more conventional in-plane Kerr magnetometry.

After the fifth data point, both saturation fields $H_s^{\perp}$ and $H_s^{\chi\perp}$ increase as the bilinear coupling changes from being ferromagnetic to antiferromagnetic. It is observed that after the fifth data point, $H_s^{\perp}$ starts to increase dramatically a few data points before $H_s^{\chi\perp}$ starts to increase. This is significant, and it will be seen later on that the resulting large difference in the values of $H_s^{\perp}$ and $H_s^{\chi\perp}$ at $d_{\mathrm{Cr}}=5$ Å (3.5 ML) is due to a peak in the biquadratic coupling at this Cr thickness. The first AFM coupling region is clearly shown by a large peak centered on about $d_{\mathrm{Cr}}=7$ Å (4.9 ML) for the plots of both $H_s^{\perp}$ and $H_s^{\chi\perp}$, in approximate agreement with the in-plane data in Fig. 1(a). The second FM coupling region can also be identified by the minimum in the plots of $H_s^{\perp}$ and $H_s^{\chi\perp}$ between about 15 and 20 Å (10.4 and 13.9 ML), again in approximate agreement with the in-plane data in Fig. 1(a). The second AFM coupling region is not well defined, however, in the plots of $H_s^{\perp}$ and $H_s^{\chi\perp}$, with the values of $H_s^{\perp}$ and $H_s^{\chi\perp}$ both increasing unexpectedly towards the end of the wedge where the Cr thickness is largest. Indeed the values of $H_s^{\perp}$ and $H_s^{\chi\perp}$ are generally much larger than expected for the Cr thicknesses after the first AFM coupling peak. It will be seen in the following section that, in addition to being sensitive to the coupling, $H_s^{\perp}$ and $H_s^{\chi\perp}$ are also sensitive to any changes that might occur in the magnetocrystalline anisotropies or in the larger (in this case) interface anisotropies as the interlayer thickness varies. This is different to the situation for in-plane Kerr measurements in which the saturation field depends only on the coupling and the relatively small magnetocrystalline anisotropies. Since the coupling is weak at large Cr thickness, the unexpected increases in $H_s^{\perp}$ and $H_s^{\chi\perp}$ are probably associated with variations in interface anisotropy with Cr thickness that are associated with the details of the structure of the Fe/Cr interface between the spacer and the upper Fe layer.

III. RELATING POLAR SATURATION FIELDS TO COUPLING CONSTANTS

It is possible to find approximate relationships between the exchange coupling strengths A_{12} and B_{12} and the saturation fields $H_s^{\perp}$ and $H_s^{\chi\perp}$ by assuming a coherent rotation model for magnetization reversal, as we shall now describe. The calculations presented here are reproduced from Ives' Ph.D. thesis (Ref. 31).

A. $H_s^{\perp}$ and coupling strengths

In order to derive the relation between the conventional perpendicular saturation field, $H_s^{\perp}$, and the coupling strength for the (001) film plane, a trilayer film is considered, consisting of magnetic layers with thicknesses d_1 and d_2 separated by a nonmagnetic interlayer. The applied magnetic field, H, is assumed to be perpendicular to the film surface. The angles between the surface normal and the directions of the magnetizations $\mathbf{M}_1$ and $\mathbf{M}_2$ are denoted by θ_1 and θ_2, where for ease of calculation the magnetizations are assumed to be confined to a plane which includes the surface normal and a fixed direction in the film plane. A schematic diagram of the system is shown in Fig. 2. The zero of θ_1 and θ_2 is assumed to be the surface normal, with both angles being allowed to vary from $-\pi$ to $+\pi$.

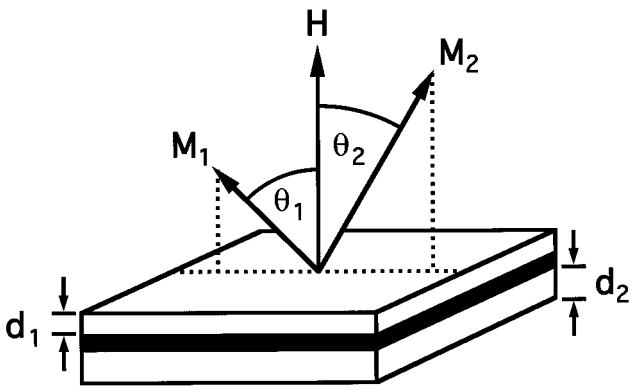

FIG. 2. A schematic diagram showing the magnetizations of the two magnetic layers and the angles they make with the field, H, applied along the film normal. The dashed lines indicate the plane which includes the surface normal and a fixed direction in the film plane, to which the magnetizations are assumed to be confined for the purposes of calculation.

The existence of any in-plane uniaxial anisotropy is ignored, but the presence of a first-order cubic anisotropy is assumed, denoted by $K_{1,j}$ for layer $j=1,2$. One of the three cubic easy axes is parallel to the film normal, while the other two are in the plane of the film. It will be assumed that for each magnetic layer, one of the in-plane cubic easy axes is aligned with the plane through the surface normal to which the magnetizations are taken to be confined. Thus the cubic anisotropy energy per unit area, for magnetization perpendicular to the plane, for a (001) surface for layer $j=1,2$, is

$$E_{\mathrm{cubic},001,j}=\frac{K_{1,j}d_J}{4}\sin^2 2\theta_j . \tag{1}$$

A demagnetizing energy per unit area for layer j, and an interface anisotropy energy per unit area are assumed, having the forms

$$E_{\mathrm{demag},j}=\frac{1}{2}\mu_0 M_j^2 d_j \cos^2\theta_j$$

and

$$E_{\mathrm{interface},j}=-2K_{i,j}\cos^2\theta_j , \tag{2}$$

where $K_{i,j}$ is the interface anisotropy constant per interface for layer j. These two terms together are equivalent to a uniaxial anisotropy with the hard-axis direction along the film normal.

The presence of both bilinear and biquadratic exchange coupling across the nonmagnetic interlayer, is assumed. For ferromagnetic layers j and $j+1$ separated by a nonmagnetic interlayer of thickness t_j, the contribution of the coupling between layers j and $j+1$ to the energy of the system per unit area is

$$E_{J,j+1}=-2A_{12}(t_j)\hat{\mathbf{M}}_j\cdot\hat{\mathbf{M}}_{j+1}-2B_{12}(t_j)(\hat{\mathbf{M}}_j\cdot\hat{\mathbf{M}}_{j+1})^2, \tag{3}$$

where $\hat{\mathbf{M}}_j$ and $\hat{\mathbf{M}}_{j+1}$ are the unit vectors of the magnetizations of layers j and $j+1$, respectively. For the moment, the coupling constants A_{12} and B_{12} will be allowed to take on any real values both positive and negative.

The general equation for the energy per unit area for a trilayer in a (001) plane for perpendicular magnetization is then

$$E=\sum_{j=1,2}\left[-\mu_0 M_j d_j H\cos\theta_j+\left(\frac{1}{2}\mu_0 M_j^2 d_j-2K_{i,j}\right)\cos^2\theta_j+\frac{K_{1,j}d_j}{4}\sin^2 2\theta_j\right]-2A_{12}\cos(\theta_1-\theta_2)-2B_{12}\cos^2(\theta_1-\theta_2). \tag{4}$$

To simplify the expressions which follow, the following substitutions will be made

$$a_j=-\mu_0 M_j d_j H,\quad b_j=\left(\frac{1}{2}\mu_0 M_j^2 d_j-2K_{i,j}\right),$$

and

$$c_j=\frac{K_{1,j}d_j}{4}. \tag{5}$$

The energy per unit area then becomes

$$E=\sum_{j=1,2}\left[a_j\cos\theta_j+b_j\cos^2\theta_j+c_j\sin^2 2\theta_j\right]-2A_{12}\cos(\theta_1-\theta_2)-2B_{12}\cos^2(\theta_1-\theta_2). \tag{6}$$

This equation may be differentiated with respect to θ_1 and θ_2, giving

$$\frac{\partial E}{\partial\theta_1}=-a_1\sin\theta_1-b_1\sin 2\theta_1+2c_1\sin 4\theta_1+2A_{12}\sin(\theta_1-\theta_2)+2B_{12}\sin 2(\theta_1-\theta_2), \tag{7}$$

$$\frac{\partial E}{\partial\theta_2}=-a_2\sin\theta_2-b_2\sin 2\theta_2+2c_2\sin 4\theta_2-2A_{12}\sin(\theta_1-\theta_2)-2B_{12}\sin 2(\theta_1-\theta_2). \tag{8}$$

Stationary points exist for $\partial E/\partial\theta_1=\partial E/\partial\theta_2=0$, and therefore for $\theta_1=\theta_2=0$. In order to determine the perpendicular saturation field, the condition which defines the field at which the stationary points at $\theta_1=\theta_2=0$ become unstable is required. This is

$$\left(\frac{\partial^2 E}{\partial\theta_1\partial\theta_2}\right)^2-\left(\frac{\partial^2 E}{\partial\theta_1^2}\right)\left(\frac{\partial^2 E}{\partial\theta_2^2}\right)=0,$$

$$\text{evaluated}\quad \text{for}\quad \theta_1=\theta_2=0. \tag{9}$$

Substitution of the second derivatives of Eq. (6) into Eq. (9), making use of Eqs. (5), and replacing H by $H_s^\perp$, leads directly to the relation

$$A_{12}+2B_{12}=-\frac{1}{2}\left[\frac{1}{\mu_0 M_1 d_1[H_s^\perp-(M_1-4K_{i,1}/\mu_0 M_1 d_1-2K_{1,1}/\mu_0 M_1)]}+\frac{1}{\mu_0 M_2 d_2[H_s^\perp-(M_2-4K_{i,2}/\mu_0 M_2 d_2-2K_{1,2}/\mu_0 M_2)]}\right]^{-1}. \tag{10}$$

The perpendicular saturation fields of layers 1 and 2 in the absence of coupling would be

$$H_{s1}^\perp=M_1-\frac{4K_{i,1}}{\mu_0 M_1 d_1}-\frac{2K_{1,1}}{\mu_0 M_1}$$

and

$$H_{s2}^\perp=M_2-\frac{4K_{i,2}}{\mu_0 M_2 d_2}-\frac{2K_{1,2}}{\mu_0 M_2},\quad (001)\ \text{only}. \tag{11}$$

Thus, provided the two magnetic layers have different saturation fields such that $H_{s1}^\perp\neq H_{s2}^\perp$, it is found from Eq. (10) that the following relation applies for both positive and negative values of A_{12} and B_{12}

$$A_{12}+2B_{12}=-\frac{1}{2}\left[\frac{1}{\mu_0 M_1 d_1(H_s^\perp-H_{s1}^\perp)}+\frac{1}{\mu_0 M_2 d_2(H_s^\perp-H_{s2}^\perp)}\right]^{-1},$$

$$(001),\ H_{s1}^\perp\neq H_{s2}^\perp,\ \text{all}\ M_1,\ \text{all}\ M_2,\ \text{all}\ d_1,\ \text{all}\ d_2,\ \text{all}\ A_{12},\ \text{all}\ B_{12}. \tag{12}$$

If the two magnetic layers have different saturation fields such that $H_{s1}^\perp\neq H_{s2}^\perp$, but equal thicknesses and magnetizations defined by $d_1=d_2=d$ and $M_1=M_2=M$, this reduces to

$$A_{12}+2B_{12}=-\frac{1}{2}\mu_0 M d\left[\frac{1}{H_s^\perp-H_{s1}^\perp}+\frac{1}{H_s^\perp-H_{s2}^\perp}\right]^{-1},\quad (001),$$

$$H_{s1}^\perp\neq H_{s2}^\perp,\ M_1=M_2,\ d_1=d_2,\ \text{all}\ A_{12},\ \text{all}\ B_{12}. \tag{13}$$

B. $H_s^{\chi\perp}$ and coupling strengths

In order to determine the initial gradient perpendicular saturation field, $H_s^{\chi\perp}=1/\chi_0$, the quantity χ_0 must be evaluated according to the definition

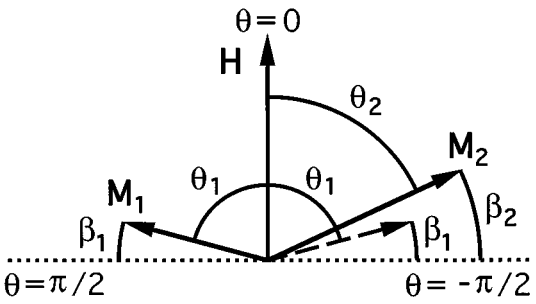

FIG. 3. Diagram showing the relationship between the large angles θ_1 and θ_2 and the small angles β_1 and β_2, for small magnetic fields applied perpendicular to the film plane. The film plane is shown by the horizontal dotted line, and the magnetizations are assumed to be confined to the plane of the page. The sizes of the angles β_1 and β_2 have been exaggerated in the diagram. The solid arrows labeled $\mathbf{M}_1$ and $\mathbf{M}_2$ show the likely arrangement of the magnetizations if both A_{12} and B_{12} are negative. The dashed arrow shows the alternative likely position of magnetization M_1 if A_{12} and B_{12} are instead positive.

$$\chi_0=\left.\frac{M_1d_1\cos\theta_1+M_2d_2\cos\theta_2}{H(M_1d_1+M_2d_2)}\right|_{H=0}. \tag{14}$$

The same energy equation as in Eq. (4) will be used here, together with the substitutions made in Eqs. (5). The first derivatives of Eq. (6), given in Eqs. (7) and (8), together with the conditions $\partial E/\partial\theta_1=\partial E/\partial\theta_2=0$, give the values of θ_1 and θ_2 corresponding to stationary points for all values of H, including those points near $H=0$ that are required for evaluating χ_0. It is not possible, however, to directly extract the exact dependences of $\cos\theta_1$ and $\cos\theta_2$ on H from these equations. It is therefore necessary to calculate approximate values of $\cos\theta_1$ and $\cos\theta_2$, using the fact that the magnetizations in the two magnetic layers make very small angles with the film plane close to $H=0$. Substitutions for θ_1 and θ_2 need to be made such that the substituted angles will have small values near $H=0$.

As above, it will be assumed that $\mathbf{M}_1$ and $\mathbf{M}_2$ are confined to a plane which includes the in-plane easy axes of the two layers and the surface normal. For positive values of H, assuming no hysteresis, $\mathbf{M}_1$ and $\mathbf{M}_2$ may therefore occupy one of two quadrants in this plane, and, according to the definitions of θ_1 and θ_2, these angles may have positive values in one quadrant and negative values in the other. In order to make appropriate substitutions for θ_1 and θ_2, it is therefore necessary to know whether $\mathbf{M}_1$ and $\mathbf{M}_2$ are in the same quadrant or in adjacent quadrants near $H=0$. If both A_{12} and B_{12} have negative values, then $\mathbf{M}_1$ and $\mathbf{M}_2$ will be in adjacent quadrants for small positive values of H, as shown in Fig. 3, and appropriate substitutions can be made for θ_1 and θ_2. This is also the case if A_{12} is negative and B_{12} is positive, since a positive B_{12} favors parallel and antiparallel alignment of the magnetizations equally, whereas a negative A_{12} favors antiparallel alignment. If both A_{12} and B_{12} have positive values, then $\mathbf{M}_1$ and $\mathbf{M}_2$ will be in the same quadrant (see Fig. 3) and substitutions can again be made. If A_{12} is positive and B_{12} is negative however, then whether $\mathbf{M}_1$ and $\mathbf{M}_2$ will be in the same quadrant or in adjacent quadrants depends on the relative magnitudes of A_{12} and B_{12} as well as on the field and the anisotropies. In this case, substitutions which would apply for all magnitudes of A_{12} and B_{12} cannot be made, and the relation between A_{12} and B_{12} and $H_s^{\chi\perp}$ cannot then be determined by this method.

If $A_{12}\geqslant 0$ and $B_{12}\geqslant 0$, the assumption that the magnetizations move within a plane which passes through the surface normal is likely to be valid in most cases and for all values of A_{12} and B_{12}. If $A_{12}\leqslant 0$ and $B_{12}\leqslant 0$, however, it can be shown, by differentiating the bilinear and biquadratic energy terms with respect to an in-plane angle between the magnetizations for all values of the out-of-plane angle, that this assumption is valid for $A_{12}\leqslant 2B_{12}\leqslant 0$ but not for values of B_{12} of greater magnitude. This restriction on the values of B_{12} allowed with this model has been verified to be correct using numerical simulations of the magnetization curves.

As illustrated in Fig. 3, the following substitutions are therefore made:

$$\theta_1=\frac{\pi}{2}-\beta_1,\quad \theta_2=\mp\frac{\pi}{2}\pm\beta_2, \tag{15}$$

where the upper signs in the second equation refer to the cases where (i) $A_{12}\leqslant 2B_{12}\leqslant 0$ or (ii) $A_{12}\leqslant 0$ and $B_{12}\geqslant 0$; the lower signs refer to the case $A_{12}\geqslant 0$ and $B_{12}\geqslant 0$; and the case where $A_{12}\geqslant 0$ and $B_{12}\leqslant 0$ is not catered for here. With these substitutions one obtains

$$\begin{aligned}
&\cos\theta_1=\cos\left(\frac{\pi}{2}-\beta_1\right)=\sin\beta_1\cong\beta_1,\\
&\cos\theta_2=\cos\left(\mp\frac{\pi}{2}\pm\beta_2\right)=\sin\beta_2\cong\beta_2,\\
&\sin2\theta_1=\sin(\pi-2\beta_1)=\sin2\beta_1\cong2\beta_1,\\
&\sin2\theta_2=\sin(\mp\pi\pm2\beta_2)=\mp\sin2\beta_2\cong\mp2\beta_2,\\
&\cos(\theta_1-\theta_2)=\cos\left[\left(\frac{\pi}{2}-\beta_1\right)-\left(\mp\frac{\pi}{2}\pm\beta_2\right)\right]\\
&\qquad\cong\mp1\pm\tfrac{1}{2}(\beta_1\pm\beta_2)^2,\\
&\cos^2(\theta_1-\theta_2)\cong\left[\mp1\pm\tfrac{1}{2}(\beta_1\pm\beta_2)^2\right]^2\cong1-(\beta_1\pm\beta_2)^2.
\end{aligned} \tag{16}$$

Using these relations in Eq. (6) leads to

$$\begin{aligned}
E=&a_1\beta_1+b_1\beta_1^2+4c_1\beta_1^2+a_2\beta_2+b_2\beta_2^2+4c_2\beta_2^2\pm2A_{12}\\
&\mp A_{12}(\beta_1\pm\beta_2)^2-2B_{12}+2B_{12}(\beta_1\pm\beta_2)^2.
\end{aligned} \tag{17}$$

Differentiation of this expression with respect to β_1 and β_2 gives

$$\begin{aligned}
\frac{\partial E}{\partial\beta_1}=&a_1+2b_1\beta_1+8c_1\beta_1\mp2A_{12}(\beta_1\pm\beta_2)\\
&+4B_{12}(\beta_1\pm\beta_2),
\end{aligned} \tag{18}$$

$$\begin{aligned}
\frac{\partial E}{\partial\beta_2}=&a_2+2b_2\beta_2+8c_2\beta_2-2A_{12}(\beta_1\pm\beta_2)\\
&\pm4B_{12}(\beta_1\pm\beta_2).
\end{aligned} \tag{19}$$

Using the fact that stationary points are given by $\partial E/\partial\beta_1 = \partial E/\partial\beta_2 = 0$, results in the following set of simultaneous equations in β_1 and β_2:

$$-a_1 = [2b_1 + 8c_1 \mp (2A_{12} \mp 4B_{12})]\beta_1 - (2A_{12} \mp 4B_{12})\beta_2,$$
$$-a_2 = [2b_2 + 8c_2 \mp (2A_{12} \mp 4B_{12})]\beta_2 - (2A_{12} \mp 4B_{12})\beta_1. \tag{20}$$

These equations are solved for β_1 and β_2, and setting $2A_{12} \mp 4B_{12} = D_{12}$, the following expressions are obtained:

$$\beta_1 = \frac{-a_1(2b_2 + 8c_2 \mp D_{12}) - a_2 D_{12}}{(2b_1 + 8c_1 \mp D_{12})(2b_2 + 8c_2 \mp D_{12}) - D_{12}^2},$$
$$\beta_2 = \frac{-a_2(2b_1 + 8c_1 \mp D_{12}) - a_1 D_{12}}{(2b_1 + 8c_1 \mp D_{12})(2b_2 + 8c_2 \mp D_{12}) - D_{12}^2}. \tag{21}$$

It is now necessary to introduce the quantities $H_{s1}^{\chi\perp}$ and $H_{s2}^{\chi\perp}$, which are equal to the saturation fields derived from the initial magnetization gradient of layers 1 and 2, respectively, in the absence of coupling. These fields are similar to the conventional saturation fields of layers 1 and 2 in the absence of coupling, $H_{s1}^{\perp}$ and $H_{s2}^{\perp}$, defined above, but differ in the sign of the term from the cubic anisotropy. They are given by

$$H_{s1}^{\chi\perp} = M_1 - \frac{4K_{i,1}}{\mu_0 M_1 d_1} + \frac{2K_{1,1}}{\mu_0 M_1}$$

and

$$H_{s2}^{\chi\perp} = M_2 - \frac{4K_{i,2}}{\mu_0 M_2 d_2} + \frac{2K_{1,2}}{\mu_0 M_2}, \quad (001) \text{ only.} \tag{22}$$

It is now possible to write

$$\begin{aligned} 2b_1 + 8c_1 &= \mu_0 M_1^2 d_1 - 4K_{i,1} + 2K_{1,1} \\ &= \mu_0 M_1 d_1 \left(M_1 - \frac{4K_{i,1}}{\mu_0 M_1 d_1} + \frac{2K_{1,1}}{\mu_0 M_1} \right) \\ &= \mu_0 M_1 d_1 H_{s1}^{\chi\perp}, \\ 2b_2 + 8c_2 &= \mu_0 M_2^2 d_2 - 4K_{i,2} + 2K_{1,2} \\ &= \mu_0 M_2 d_2 \left(M_2 - \frac{4K_{i,2}}{\mu_0 M_2 d_2} + \frac{2K_{1,2}}{\mu_0 M_2} \right) \\ &= \mu_0 M_2 d_2 H_{s2}^{\chi\perp}. \end{aligned} \tag{23}$$

Using the fact that $-a_1 = \mu_0 M_1 d_1 H$ and $-a_2 = \mu_0 M_2 d_2 H$, and writing $\mu_1 = M_1 d_1$ and $\mu_2 = M_2 d_2$, Eqs. (21) can be written as

$$\beta_1 = H\,\frac{\mu_0^2 \mu_1 \mu_2 H_{s2}^{\chi\perp} \mp D_{12}\mu_0\mu_1 + D_{12}\mu_0\mu_2}{(\mu_0\mu_1 H_{s1}^{\chi\perp} \mp D_{12})(\mu_0\mu_2 H_{s2}^{\chi\perp} \mp D_{12}) - D_{12}^2},$$
$$\beta_2 = H\,\frac{\mu_0^2 \mu_1 \mu_2 H_{s1}^{\chi\perp} \mp D_{12}\mu_0\mu_2 + D_{12}\mu_0\mu_1}{(\mu_0\mu_1 H_{s1}^{\chi\perp} \mp D_{12})(\mu_0\mu_2 H_{s2}^{\chi\perp} \mp D_{12}) - D_{12}^2}. \tag{24}$$

The initial gradient saturation field $H_s^{\chi\perp}$ can now be evaluated, which, from the definition in Eq. (14), is given by

$$H_s^{\chi\perp} = \frac{1}{\chi_0} = \left.\frac{H(\mu_1 + \mu_2)}{\mu_1\beta_1 + \mu_2\beta_2}\right|_{H=0}, \tag{25}$$

and becomes

$$H_s^{\chi\perp} = \frac{(\mu_1 + \mu_2)[\mu_0\mu_1\mu_2 H_{s1}^{\chi\perp} H_{s2}^{\chi\perp} \mp (2A_{12} \mp 4B_{12})(\mu_1 H_{s1}^{\chi\perp} + \mu_2 H_{s2}^{\chi\perp})]}{\mu_0\mu_1\mu_2(\mu_2 H_{s1}^{\chi\perp} + \mu_1 H_{s2}^{\chi\perp}) \mp (2A_{12} \mp 4B_{12})(\mu_1 \mp \mu_2)^2}. \tag{26}$$

Rearranging this equation gives

$$A_{12} \mp 2B_{12} = \pm \frac{\frac{1}{2}\mu_0\mu_1\mu_2[H_s^{\chi\perp}(\mu_2 H_{s1}^{\chi\perp} + \mu_1 H_{s2}^{\chi\perp}) - H_{s1}^{\chi\perp} H_{s2}^{\chi\perp}(\mu_1 + \mu_2)]}{H_s^{\chi\perp}(\mu_1 \mp \mu_2)^2 - (\mu_1 + \mu_2)(\mu_1 H_{s1}^{\chi\perp} + \mu_2 H_{s2}^{\chi\perp})},$$
$$(001);\ H_{s1}^{\chi\perp} \neq H_{s2}^{\chi\perp};\ \text{all } M_1,\ M_2;\ \text{all } d_1,\ d_2;$$
$$\text{upper sign } (i)\ A_{12} \leqslant 2B_{12} \leqslant 0,\ (ii)\ A_{12} \leqslant 0 \text{ and } B_{12} \geqslant 0;\ \text{lower sign } A_{12} \geqslant 0 \text{ and } B_{12} \geqslant 0. \tag{27}$$

If the two magnetic layers have equal thicknesses and magnetizations so that $\mu_1 = \mu_2 = \mu$, but different values of $K_{i,j}$ or $K_{1,j}$, then for the case $A_{12} \leqslant 0$, Eq. (27) reduces to

$$A_{12} - 2B_{12} = -\tfrac{1}{4}\mu_0 M d \left(H_s^{\chi\perp} - \frac{2H_{s1}^{\chi\perp} H_{s2}^{\chi\perp}}{H_{s1}^{\chi\perp} + H_{s2}^{\chi\perp}} \right), \quad (001),$$
$$H_{s1}^{\chi\perp} \neq H_{s2}^{\chi\perp},\ M_1 = M_2,\ d_1 = d_2,$$
$$(i) A_{12} \leqslant 2B_{12} \leqslant 0,\ (ii) A_{12} \leqslant 0 \text{ and } B_{12} \geqslant 0. \tag{28}$$

BLS measurements and polar Kerr magnetization curves, performed on the trilayer at a Cr thickness corresponding to extremely small exchange coupling between the Fe layers, when taken together suggested that the thicknesses and magnetizations of the two Fe layers were identical, as expected, but that the two Fe layers possessed different interface anisotropies. This meant that the conventional perpendicular saturation fields, $H_{s1}^{\perp}$ and $H_{s2}^{\perp}$, of the individual Fe layers in the absence of coupling, were not quite the same, and that the initial gradient saturation field, $H_{s1}^{\chi\perp}$ and $H_{s2}^{\chi\perp}$, of the individual layers in the absence of coupling, were also not identical. Thus in this case the appropriate relation between the conventional perpendicular saturation field $H_s^{\perp}$ and the coupling strengths is given by Eq. (13), while the appropriate relation between the initial gradient perpendicular saturation

field $H_s^{\chi\perp}$ and the coupling strengths, for either $A_{12} \leqslant 2B_{12} \leqslant 0$ or $A_{12} \leqslant 0$ and $B_{12} \geqslant 0$, is given by Eq. (28). From those equations it can be seen that the saturation fields $H_s^{\perp}$ and $H_s^{\chi\perp}$ will in general both have a nonlinear dependence on the coupling strengths, and since the values of $H_{s1}^{\perp}$, $H_{s2}^{\perp}$, $H_{s1}^{\chi\perp}$, and $H_{s2}^{\chi\perp}$ are not known, evaluation of A_{12} and B_{12} from Eqs. (13) and (28) is virtually impossible.

A reasonable estimate of A_{12} and B_{12} can however be made, by making the approximation that the two Fe layers are identical. With this assumption $H_{s1}^{\perp} = H_{s2}^{\perp}$, $H_{s1}^{\chi\perp} = H_{s2}^{\chi\perp}$, and so

$$H_s^{\perp} = H_{s1}^{\perp} - \frac{4}{\mu_0 M d}(A_{12} + 2B_{12}), \tag{29}$$

$$H_s^{\chi\perp} = H_{s1}^{\chi\perp} - \frac{4}{\mu_0 M d}(A_{12} - 2B_{12}). \tag{30}$$

The expressions for $H_{s1}^{\perp}$ and $H_{s1}^{\chi\perp}$, which were given in Eqs. (11) and (22), depend on the magnetocrystalline and interface anisotropies of the magnetic layers, and on demagnetizing effects. In theory these quantities would be expected to be independent of any changes in nonmagnetic interlayer thickness and could be calculated for a particular sample. For a sample such as the Fe/Cr/Fe trilayer studied here, however, we have found that $H_{s1}^{\perp}$ and $H_{s1}^{\chi\perp}$ are not entirely independent of the Cr interlayer thickness, which we believe is due to a variation of the interface anisotropy with Cr thickness, and as a consequence $H_{s1}^{\perp}$ and $H_{s1}^{\chi\perp}$ cannot be calculated with sufficient accuracy to allow the coupling to be deduced.

In order to estimate values for the coupling strengths, values of $H_{s1}^{\perp}$ and $H_{s1}^{\chi\perp}$ can be chosen from the plots of $H_s^{\perp}$ and $H_s^{\chi\perp}$ versus Cr thickness, and this has been done in two steps. The first step is to consider that if the cubic anisotropy, which causes a small curvature in the magnetization curves, is ignored, the values of $H_s^{\perp}$ and $H_s^{\chi\perp}$ should be equal at the point just before the Cr wedge begins since no interlayer coupling can exist at this point. The plots of $H_s^{\perp}$ and $H_s^{\chi\perp}$ have thus been shifted in field relative to each other until they coincide at $d_{\mathrm{Cr}} = 0$.

The second step is to produce a plot of normalized saturation fields so that for $d_{\mathrm{Cr}} > 0$ the values of the normalized fields are in theory due to coupling only. If the normalized perpendicular saturation fields are defined by $\Delta H_s^{\perp}$ and $\Delta H_s^{\chi\perp}$, then

$$\Delta H_s^{\perp} = H_s^{\perp} - H_{s1}^{\perp} = -\frac{4}{\mu_0 M d}(A_{12} + 2B_{12}), \tag{31}$$

$$\Delta H_s^{\chi\perp} = H_s^{\chi\perp} - H_{s1}^{\chi\perp} = -\frac{4}{\mu_0 M d}(A_{12} - 2B_{12}). \tag{32}$$

Since the result of step 1 is that the smallest value of $H_s^{\chi\perp}$ is below that of $H_s^{\perp}$, the second step is achieved by putting

$$H_{s1}^{\perp} = H_{s1}^{\chi\perp} = (\text{smallest observed value of } H_s^{\chi\perp}). \tag{33}$$

The plots of the normalized saturation fields $\Delta H_s^{\perp}$ and $\Delta H_s^{\chi\perp}$ are thus obtained in this case by subtracting the smallest observed value of $H_s^{\chi\perp}$ from the plots of both $H_s^{\perp}$ and $H_s^{\chi\perp}$. The plots of the normalized saturation fields $\Delta H_s^{\perp}$ and $\Delta H_s^{\chi\perp}$ are shown in Fig. 1(c).

Values of A_{12} may then be estimated by adding the plots of $\Delta H_s^{\perp}$ and $\Delta H_s^{\chi\perp}$, while values of B_{12} may be estimated, in principle, by subtracting the plot of $\Delta H_s^{\chi\perp}$ from that of $\Delta H_s^{\perp}$ according to

$$A_{12} = -\frac{\mu_0 M d}{8}(\Delta H_s^{\perp} + \Delta H_s^{\chi\perp}), \tag{34}$$

$$B_{12} = -\frac{\mu_0 M d}{16}(\Delta H_s^{\perp} - \Delta H_s^{\chi\perp}). \tag{35}$$

These equations are only valid for $A_{12} \leqslant 2B_{12} \leqslant 0$ or $A_{12} \leqslant 0$ and $B_{12} \geqslant 0$, as explained above. The region we are most interested in is that of the first AFM coupling peak however, in which A_{12} is negative and the condition $|A_{12}| \geqslant |2B_{12}|$ is well satisfied in our data. This means that we can only strictly rely on the values of A_{12} and B_{12} obtained using Eqs. (34) and (35) for Cr thicknesses in the range 3 to 15 Å, which is the range of the first AFM coupling region shown by the polar Kerr measurements in Fig. 1(b).

IV. COUPLING BEHAVIOR DEDUCED FROM POLAR KERR MAGNETOMETRY

In Fig. 4(a), the values of A_{12} estimated from polar Kerr measurements using Eq. (34) are plotted versus Cr thickness. The first bilinear coupling peak at about $d_{\mathrm{Cr}} = 7$ Å (4.9 ML) can be clearly seen in Fig. 4(a). The second bilinear peak, although out of range of the validity of our theoretical interpretation using Eq. (34) which applies for $3 \leqslant d_{\mathrm{Cr}} \leqslant 15$ Å, is anyway obscured by the increase in the saturation fields occurring towards larger Cr thicknesses believed to be caused by variations in interface anisotropies with Cr thickness.

The bilinear and biquadratic coupling strengths estimated from in-plane Kerr and BLS measurements were described in detail in Ref. 26, but are reproduced again in Figs. 4(b) and 5(b) for comparison with the polar Kerr data. From Fig. 4(b), the maximum bilinear coupling strength appears to occur at about $d_{\mathrm{Cr}} = 7$ Å, having the value -0.15 mJ m^{-2} at this point. In comparison, a somewhat larger maximum value of $A_{12} = -0.21$ mJ m^{-2}, estimated from the peak at 7 Å in Fig. 4(a), is obtained using polar Kerr magnetometry, and the difference would appear to result from the underlying increase in the polar Kerr plot of A_{12} with increasing Cr thickness. These values for the bilinear coupling strength are much smaller than those obtained by some other researchers,[8,16,32,33] however, and it is believed that increased roughness at the Fe-Cr interfaces may be responsible for attenuating the total (bilinear plus biquadratic) coupling strength in our sample. Heinrich *et al.*[10] have shown that the overall coupling strength is strongly affected by the growth temperature, being greater for higher growth temperatures. This indicates that the reduced coupling strength in our samples is due to the growth at room temperature of the Fe/Cr/Fe structure, as opposed to the higher growth temperatures used by other research groups.

From Fig. 5(b) it is seen that the biquadratic coupling strength B_{12} estimated from in-plane Kerr magnetometry and

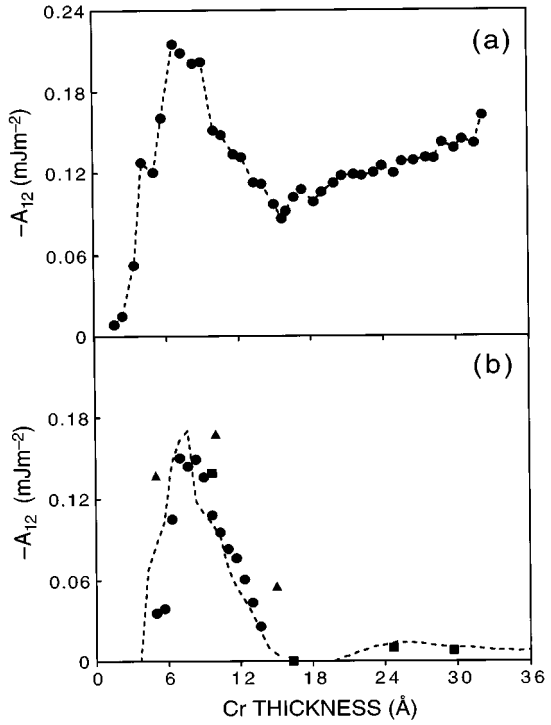

FIG. 4. (a) Shown plotted as a function of Cr thickness are the values of A_{12} as deduced from the normalized perpendicular saturation field plots in Fig. 1(c). (b) The values of A_{12} as deduced from in-plane Kerr magnetometry (circles), from BLS (squares), and from BLS on a second trilayer with $0 \leqslant d_{Cr} \leqslant 20$ Å (triangles) are plotted versus Cr thickness for comparison. The dashed curve is a scaled version of the curve in Fig. 1(a) and serves only to guide the eye.

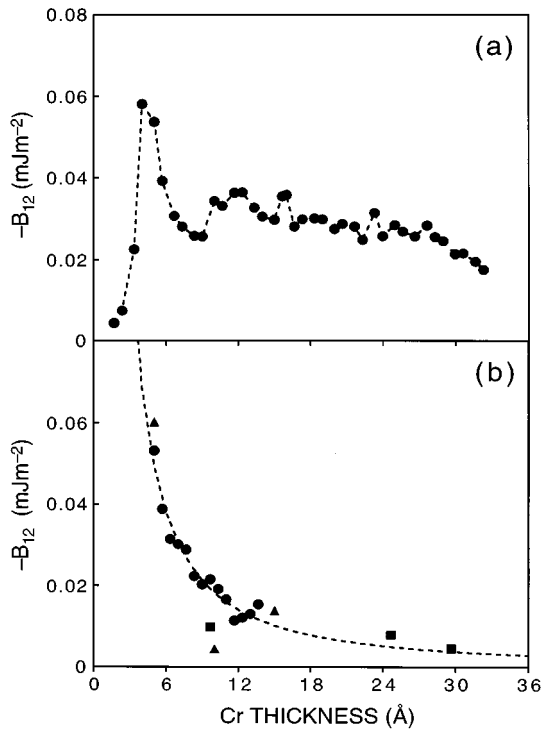

FIG. 5. (a) Shown plotted as a function of Cr thickness are the values of B_{12} as deduced from the normalized perpendicular saturation field plots in Fig. 1(c). (b) The values of B_{12} as deduced from in-plane Kerr magnetometry (circles), from BLS (squares), and from BLS on a second trilayer with $0 \leqslant d_{Cr} \leqslant 20$ Å (triangles) are plotted versus Cr thickness for comparison. The dashed curve is a $d_{Cr}^{-1.4}$ fit to the data.

BLS is largest at a Cr thickness of about 5 Å (3.5 ML) and decreases for larger Cr thicknesses, approximately following a $d_{Cr}^{-1.4}$ dependence for Cr thicknesses between 5 and 30 Å (3.5 and 20.8 ML). The fluctuation of some data points, however, in particular around $d_{Cr}=10$ Å (6.9 ML), means that the existence of oscillations in B_{12} are not ruled out by the in-plane Kerr and BLS measurements. In Fig. 5(a), the values of B_{12} estimated from polar Kerr measurements using Eq. (35) are plotted versus Cr thickness. It was observed above when the polar Kerr saturation fields $H_s^{\perp}$ and $H_s^{\chi\perp}$ were plotted in Fig. 1(b) that after the fifth data point $H_s^{\perp}$ started to increase dramatically a few data points before $H_s^{\chi\perp}$ started to increase. This resulted in a large difference in the values of $H_s^{\perp}$ and $H_s^{\chi\perp}$ at $d_{Cr}=5$ Å. Thus when $\Delta H_s^{\chi\perp}$ is subtracted from $\Delta H_s^{\perp}$ in Eq. (35) to obtain an estimate of B_{12}, a peak is observed in the plot of B_{12} versus Cr thickness at $d_{Cr}=5$ Å, which can be clearly seen in Fig. 5(a). This peak occurs in almost exactly the same place as the maximum value of B_{12} observed using in-plane Kerr magnetometry and BLS in Fig. 5(b), and also its magnitude is almost exactly the same as that of the peak in B_{12} in Fig. 5(b).

The plot of B_{12} estimated from polar Kerr measurements suggests that before the peak at 5 Å (3.5 ML), B_{12} increases from zero near zero Cr thickness. It also suggests that after the peak at 5 Å there is a trough at $d_{Cr}=8$ Å (5.6 ML) followed by a second peak in B_{12} at $d_{Cr}=12$ Å (8.3 ML), which is evidence that B_{12} falls off in an oscillatory fashion with increasing Cr thickness. For Cr thicknesses outside the range $3 \leqslant d_{Cr} \leqslant 15$ Å the plot is strictly invalid due to the limitations put on A_{12} in the theory. Also, the values of B_{12} shown for the larger Cr thicknesses are not reliable, unlike those shown for lower thicknesses, because of the increases that were observed in the saturation fields at larger Cr thicknesses. Above 15 Å however, the plot of B_{12} estimated from polar Kerr measurements does suggest a much more gradual falloff than the approximate $d_{Cr}^{-1.4}$ dependence of B_{12} in Fig. 5(b).

It should be noted that the absolute values of A_{12} and B_{12} presented in Figs. 4(a) and 5(a) are subject to some extent to the method chosen for normalizing the saturation field plots of $H_s^{\perp}$ and $H_s^{\chi\perp}$ in Fig. 1(b). A different method of normalization would result in all the values of A_{12} and all the values of B_{12} having a constant value added or subtracted to them, although the shape of the plots of A_{12} and B_{12} would remain unchanged.

V. CONCLUSION

To summarize, the polar Kerr measurements described here strongly suggested an oscillatory behavior for the biquadratic coupling as a function of Cr thickness in the range $d_{Cr}=3$ to 15 Å. The in-plane Kerr and BLS measurements, described in Ref. 26, suggested a $d_{Cr}^{-1.4}$ thickness dependence for the biquadratic coupling for Cr thicknesses greater than the maximum value at 5 Å (3.5 ML), but the fluctuation of

some data points did not rule out the presence of oscillations. The polar Kerr measurements also clearly indicated a peak in the biquadratic coupling at $d_{Cr}=5$ Å, having the same peak height as that observed using in-plane Kerr magnetometry and BLS. The polar Kerr measurements suggested additionally that B_{12} increases monotonically from zero near zero Cr thickness to the maximum at 5 Å. They also suggested that after the peak at 5 Å there is a trough at $d_{Cr}=8$ Å (5.6 ML) followed by a second peak in B_{12} at $d_{Cr}=12$ Å (8.3 ML), which is evidence that B_{12} falls off in an oscillatory fashion. The polar Kerr data at higher Cr thicknesses was not thought to be so reliable because of the increases in the saturation field data at these thicknesses which were thought to be due to a variation of interface anisotropy with Cr thickness, and this data was also outside the range of $3 \leqslant d_{Cr} \leqslant 15$ Å for which our theoretical interpretation was valid.

We now compare the coupling behavior observed for our Fe/Cr/Fe trilayer with that reported by Köbler *et al.*[16] The maximum value of A_{12} reported by Köbler *et al.* was -0.50 mJ m^{-2}, which occurred at $d_{Cr}=7$ Å (4.9 ML). This value of A_{12} is 3.3 times greater in magnitude than the maximum value of $A_{12}=-0.15$ mJ m^{-2} obtained from Fig. 4(b) from in-plane Kerr magnetometry and BLS [more reliable than the maximum value from Fig. 4(a)], but it is interesting that the position of the maximum of A_{12} reported by Köbler *et al.* is the same as the position of the maximum in Figs. 4(a) and 4(b) which is $d_{Cr}=7$ Å. The maximum value of B_{12} reported by Köbler *et al.* was -0.21 mJ m^{-2}, and this occurred at a Cr thickness of 6 Å (4.2 ML). This value of B_{12} is 3.5 times greater in magnitude than the maximum value of $B_{12}=-0.06$ mJ m^{-2} obtained for our Fe/Cr/Fe trilayer from both the polar Kerr measurements in Fig. 5(a) and the in-plane Kerr and BLS measurements in Fig. 5(b). The position of the maximum in B_{12} reported by Köbler *et al.* is however very similar to the position of the maximum in Figs. 5(a) and 5(b) which is $d_{Cr}=5$ Å (3.5 ML). There are no values of A_{12} or B_{12} given for Cr thicknesses less than 6 Å in the paper by Köbler *et al.*, so we cannot compare the behavior of B_{12} in their sample with the behavior of B_{12} suggested by the polar Kerr measurements in this low Cr thickness range. For Cr thicknesses between 6 and 16 Å (4.2 and 11.1 ML), however, there is some evidence of a gradually decaying oscillatory behavior in their values of B_{12} with increasing Cr thickness, which is essentially the behavior observed here using polar Kerr magnetometry in this thickness region. A second maximum in the value of B_{12} is seen by them at about $d_{Cr}=13$ Å (9.0 ML), whereas a second maximum is observed in Fig. 5(a) at a similar thickness of $d_{Cr}=12$ Å (8.3 ML). Apart from a scaling factor of approximately 3.4, probably caused by the greater amount of interface roughness in our sample, the behavior of the coupling strengths that is reported by Köbler *et al.* is thus very similar to some of the polar Kerr data reported here, and the ratio of the maximum value of B_{12} to the maximum value of A_{12} has the same value here as in Ref. 16, about 0.41.

Finally, we compare the coupling behavior observed here with that predicted theoretically by Edwards, Ward, and Mathon[17] using an intrinsic model to obtain the biquadratic coupling. In Ref. 17, a plot showing how A_{12} and B_{12} are both expected to oscillate as a function of spacer thickness gives the height of the first maximum in B_{12} to be 0.56 of the height of the first maximum in A_{12}, which compares quite favorably with the ratio of 0.41 found in this work. The position of the first maximum in B_{12} is shown in the theoretical plot in Ref. 17 to occur at a spacer thickness equal to half the spacer thickness at which the first maximum occurs in the plot of A_{12}. This is quite similar to the ratio of 0.71 arising from the positions of $d_{Cr}=5$ Å (3.5 ML) and $d_{Cr}=7$ Å (4.9 ML) observed here for the first biquadratic and bilinear coupling peaks, respectively.

The second maximum of B_{12} in the theoretical plot of Ref. 17 occurs just before the bilinear coupling crosses over from antiferromagnetic to ferromagnetic, as the Cr thickness increases beyond the first maximum in A_{12}, which is also the case for our plot of B_{12} from the polar Kerr measurements in Fig. 5(a). The height of the second maximum in B_{12} in Ref. 17 is, however, a significantly smaller fraction of the height of the first maximum in B_{12} in Ref. 17 than is our second maximum in B_{12} in Fig. 5(a) as a fraction of the corresponding first maximum in B_{12}. The very rapid decay of the biquadratic coupling strength with spacer thickness in the Edwards model, contrasting with the less rapid decay observed here and by Köbler *et al.*,[16] may result from the fact that the model used in Ref. 17 was quite a simple one, and more advanced theories of the biquadratic coupling may resolve such discrepancies. Nevertheless, the fact that the Edwards theory, like many other theories of the biquadratic exchange coupling,[15,16] predicts that B_{12} should decay with interlayer thickness in an oscillatory fashion, tends to support the results from the polar Kerr measurements in Fig. 5(a).

ACKNOWLEDGMENTS

We would like to thank S. J. Gray and M. Gester for growing the Fe/Cr/Fe trilayer and to acknowledge financial support from the EPSRC and the Toshiba Corporation.

[1] P. Grünberg, R. Schreiber, Y. Pang, M. Brodsky, and H. Sowers, Phys. Rev. Lett. **57**, 2442 (1986).

[2] Y. Wang, P. M. Levy, and J. L. Fry, Phys. Rev. Lett. **65**, 2732 (1990).

[3] E. Fawcett, Rev. Mod. Phys. **60**, 209 (1988).

[4] J. Unguris, R. J. Celotta, and D. T. Pierce, Phys. Rev. Lett. **67**, 140 (1991).

[5] S. T. Purcell, W. Folkerts, M. T. Johnson, N. W. E. McGee, K. Jager, J. van de Stegge, W. B. Zeper, and W. Hoving, Phys. Rev. Lett. **67**, 903 (1991).

[6] J. Unguris, R. J. Celotta, and D. T. Pierce, Phys. Rev. Lett. **69**, 1125 (1992).

[7] E. E. Fullerton, M. J. Conover, J. E. Mattson, C. H. Sowers, and S. D. Bader, Phys. Rev. B **48**, 15 755 (1993).

[8] B. Heinrich, M. From, J. F. Cochran, L. X. Liao, Z. Celinski, C. M. Schneider, and K. Myrtle, in *Magnetic Ultrathin Films, Mul-*

tilayers and Surfaces/Interfaces, and Characterization, edited by B. T. Jonker *et al.*, MRS Symposia Proceedings No. 313 (Materials Research Society, Pittsburgh, 1993), p. 119.
[9] A. Davies, J. A. Stroscio, D. T. Pierce, and R. J. Celotta, Phys. Rev. Lett. **76**, 4175 (1996).
[10] B. Heinrich, J. F. Cochran, D. Venus, K. Totland, C. Schneider, and K. Myrtle, J. Magn. Magn. Mater. **156**, 215 (1996).
[11] D. Stoeffler and F. Gautier, Phys. Rev. B **44**, 10 389 (1991).
[12] M. Rührig, R. Schäfer, A. Hubert, R. Mosler, J. A. Wolf, S. Demokritov, and P. Grünberg, Phys. Status Solidi A **125**, 635 (1991).
[13] A. Fuss, S. Demokritov, P. Grünberg, and W. Zinn, J. Magn. Magn. Mater. **103**, L221 (1992).
[14] Z. Celinski, B. Heinrich, and J. F. Cochran, J. Magn. Magn. Mater. **145**, L1 (1995).
[15] B. Rodmacq, K. Dumesnil, P. Mangin, and M. Hennion, Phys. Rev. B **48**, 3556 (1993).
[16] U. Köbler, K. Wagner, R. Wiechers, A. Fuss, and W. Zinn, J. Magn. Magn. Mater. **103**, 236 (1992).
[17] D. M. Edwards, J. M. Ward, and J. Mathon, J. Magn. Magn. Mater. **126**, 380 (1993).
[18] J. Barnaś, J. Magn. Magn. Mater. **123**, L21 (1993).
[19] R. P. Erickson, K. B. Hathaway, and J. R. Cullen, Phys. Rev. B **47**, 2626 (1993).
[20] P. Bruno, J. Magn. Magn. Mater. **121**, 248 (1993).
[21] J. C. Slonczewski, J. Magn. Magn. Mater. **126**, 374 (1993).
[22] S. Demokritov, E. Tsymbal, P. Grünberg, W. Zinn, and I. K. Schuller, Phys. Rev. B **49**, 720 (1994).
[23] J. C. Slonczewski, Phys. Rev. Lett. **67**, 3172 (1991).
[24] J. C. Slonczewski, J. Appl. Phys. **73**, 5957 (1993).
[25] M. E. Filipkowski, J. J. Krebs, G. A. Prinz, and C. J. Gutierrez, Phys. Rev. Lett. **75**, 1847 (1995).
[26] R. J. Hicken, C. Daboo, M. Gester, A. J. R. Ives, S. J. Gray, and J. A. C. Bland, J. Appl. Phys. **78**, 6670 (1995).
[27] D. T. Pierce, J. A. Stroscio, J. Unguris, and R. J. Celotta, Phys. Rev. B **49**, 14 564 (1994).
[28] A. J. R. Ives, J. A. C. Bland, T. Thomson, P. C. Riedi, M. J. Walker, J. Xu, and D. Greig, J. Magn. Magn. Mater. **154**, 301 (1996).
[29] A. J. R. Ives, R. J. Hicken, J. A. C. Bland, C. Daboo, M. Gester, and S. J. Gray, J. Appl. Phys. **75**, 6458 (1994).
[30] C. Turtur, G. Bayreuther, Phys. Rev. Lett. **72**, 1557 (1994).
[31] A. J. R. Ives, Ph. D. thesis, University of Cambridge, United Kingdom, 1995.
[32] P. Grünberg, A. Fuss, Q. Leng, R. Schreiber, and J. A. Wolf, *Magnetism and Structure in Systems of Reduced Dimension*, NATO Advanced Study Institute, Series B Physics (Plenum, New York, 1992).
[33] S. Demokritov, J. A. Wolf, and P. Grünberg, Europhys. Lett. **15**, 881 (1991).